Metallopyrrole-Capped Carbon Nanocones

Stanislav R. Stoyanov and Petr Král*

Department of Chemistry, University of Illinois at Chicago, Chicago, Illinois 60607

Received: April 18, 2006; In Final Form: August 22, 2006

We design nickel-doped and nitrogen-doped carbon nanocones with various amounts of buckling that feature square-planar, (approximate) tetrahedral, and octahedral coordination. The optimized geometries and electronic structures of these novel metallocarbon complexes are calculated by using the B3LYP (Gaussian03) and GGA-BLYP (ADF) exchange-correlation functionals. We analyze buckling and stability of the nanocones, and discuss their potential for additional functionalization at the metallic site.

Introduction

Carbon fullerenes,[1] nanotubes,[2] nanocones,[3] and their endless hybrids possess unique material properties, such as mechanical rigidity and electronic conduction, due to their rich $\pi-\pi$ binding.[4] Carbon nanostructures can also form many types of hybrid nanodevices.[5] If such structures are equipped at *predesigned* binding sites with functional moieties, they might be able to perform novel controllable chemical, electronic, and mechanical activities.

Numerous studies show that although most carbon nanostructures are mechanically and chemically very stable, they can be modified by physisorption[6] or covalent bonding.[7] Carbon nanocones with "open" pocket-like structures and "spike-like" tips might be especially suitable for functionalization leading to rich potential applications. Their tips have been, for example, functionalized by oxidation and subsequent deposition of Gd atoms.[8] It would be particularly interesting to design universal binding sites in C nanocones and other nanostructures, allowing controllable connection of various ligands.

We address this problem by turning our attention to *metalloporphyrins*, which gain their universality from a central metal site coupled to several loosely connected pyrrole rings.[9] Metalloporphyrins, with Fe in different oxidation states, can easily undergo redox reactions in living systems and activate many biochemical reactions.[10,11] Porphyrins can be part of square planar as well as octahedral complexes, whose structures have been thoroughly investigated.[12,13] Recently, porphyrin-based nanostructures, such as nanotapes[14] or nanochannels,[15] have also been discussed.

In this work, we theoretically examine the possibility of "integrating" metalloporphyrins into carbon nanostructures, with the goal of forming novel types of binding sites for their potential functionalization. These structures are obtained by substituting several C atoms by N atoms, and coordinating them to a central transition metal ion.

Design of the Structures

In Figure 1, we present a series of Ni(II) and nitrogen-doped carbon nanocones that are calculated by ab initio techniques described below. The structures have been obtained by stepwise modifications of metalloporphyrins, leading to carbon nanocones with integrated metal binding sites. In analogy to elementary cells in carbon nanotubes (CNTs), we can introduce layers in such structures: the first is the metal, the second contains the N atoms, the third has the C atoms connected to them and to their next C atom neighbors, etc. We consider the following modifications of metalloporphyrins:

(i) The metalloporphyrin **1** can be "frustrated" in the third layer, where we remove the four methine C atoms. As a result, we obtain structure **2** that is buckled, since the methine linkers

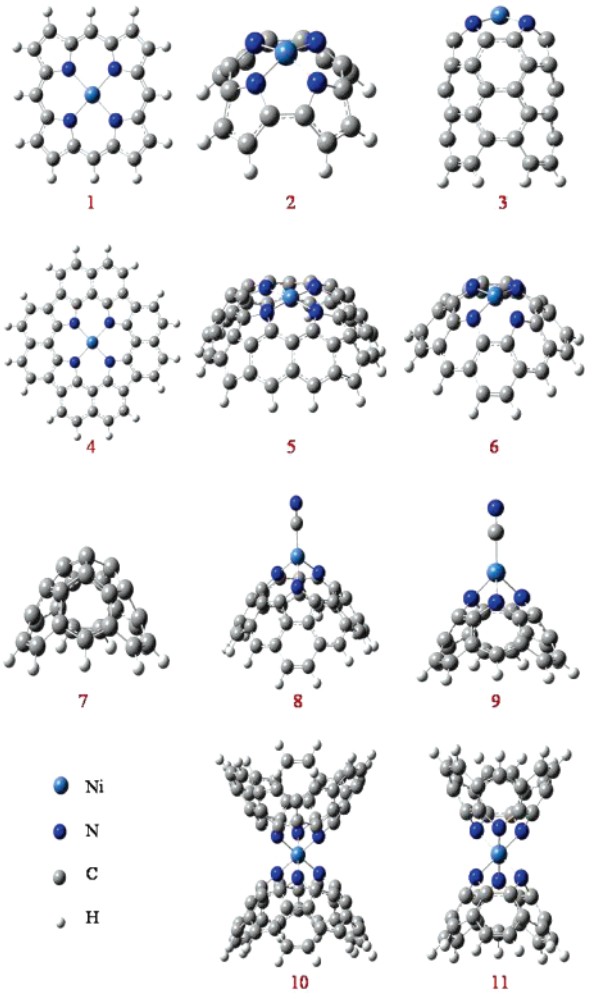

Figure 1. Carbon nanocones doped with Ni(II) and N atoms. Structures **1**−**6** are in the first group whereas **7**−**11** are in the second group.

* Address correspondence to this author. E-mail: pkral@uic.edu.

10.1021/jp062387j CCC: $33.50
Published on Web 10/10/2006

between its four pyrrole rings are removed. The structure is terminated by an "armchair" rim, allowing it to be closed by another cone or to be connected to the (4,4) CNT, as shown in **3**.

(ii) The porphyrin structure **1** can also be "extended" by completing eight benzene rings fused to four pyrrole rings. This creates the flat structure **4**.

(iii) In nanocone **5**, we close the fourth layer of structure **4**, by adding four more C atoms. The obtained structure buckles, but the resulting tension is relatively small. The cone gains a "zigzag" rim, fitting the (12,0) nanotube.

(iv) We can also combine the frustration and extension of the metalloporphyrin **1**, as shown in the cone **6**, where the methine linkers are removed and the five-membered pyrrole rings are substituted with six-membered pyridine rings. Structure **6** is fully based on the 120° carbon nanocone and differs from it in *four* N−C substitutions, and a closure with a Ni atom instead of *two* C atoms.

(v) To modify a 180° carbon nanocone, such as **7**, the metalloporphyrin is frustrated by a pyrrole defect, as shown in **8** and **9**. Structure **9** differs from structure **7** in *three* N−C substitutions and closure with a Ni atom instead of *one* C atom. Complexes **8** and **9** are analogous in structure to **5** and **6**, respectively. Complexes **5** and **8** contain pyrrole N atoms, whereas **6** and **9** contain pyridine N atoms. However, cones **8** and **9** are sharper than **5** and **6**, and form tetrahedral as well as octahedral complexes. The four-coordinate (approximate tetrahedral) complexes **8** and **9** are completed here by cyanide ligands. The octahedral complexes **10** and **11** are formed by the binding of two cones to one metal atom.

All these metallo-capped cones can be continued by adding more C atom rings, in such a way that they follow the structure of typical carbon nanocones.[3] Moreover, their rims could be arranged to fit either zigzag or armchair tips of nanotubes, depending on the layer where we perform their frustration.

Computational Technique

We describe the structure and electronic properties of these complexes using Density Functional Theory (DFT) that has proven to be a powerful tool for investigation of transition metal complexes.[16] We calculate the optimized geometries and electronic structures of the complexes in Figure 1, using the B3LYP exchange-correlation functional, incorporated in the Gaussian03 software package (G03).[17] For all the atoms, we use the all-electron triple-ζ 6-311G* basis set. The atomic charges and the Wiberg bond orders are calculated by using Natural Bond Orbital (NBO).[18] For comparison, we perform optimizations of these structures also with the Amsterdam Density Functional (ADF),[19] where we use the Generalized Gradient Approximation (GGA) and the BLYP exchange-correlation functional. For all the atoms, we utilize the TZP basis set that is similar to the triple-ζ 6-311G* in Gaussian03.

Results and Discussion

In this study, we use Ni(II) because it forms stable square planar, tetrahedral, and octahedral complexes. We treat the studied complexes shown in Figure 1 as neutral, in analogy to Ni(II)porphyrin. They can be divided into two groups, depending on the number of coordinating N atoms of the nanocone ligand (NL). The square planar complexes **1**−**6** that contain tetradentate NLs comprise the first group. Complexes **8**−**11** that contain tridentate NLs are in the second group. The four-coordinate complexes **8** and **9** contain one tridentate NL and one cyanide ligand, while the octahedral complexes **10** and **11** contain two identical tridentate NLs.

TABLE 1: Selected Optimized N−N Distances for Anionic Ligands (N−N(L)) and for Complexes (N−N(cx)) and Ni−N Distances (Å), N−Ni−N Angles (deg), and Natural Ni Atom Charges (q(Ni)) for the Complexes in Their Ground Electronic States (GS)[a]

complex	GS	N−N(cx)	N−N(L)	Ni−N	N−Ni−N	q(Ni)
1	singlet	3.94	4.17	1.97	90.0	1.17
2	singlet	3.56	3.75	1.83	87.1	1.00
3	singlet	3.74	3.99	1.92	87.5	1.09
4	triplet	3.91	4.09	1.96	90.0	1.19
5	singlet	4.00	4.39	2.00	89.8	1.18
6	singlet	3.57	3.68	1.83	87.5	1.07
7	doublet					
8	quintet	2.69	2.68	1.97	86.2	1.38
9	quartet	2.52	2.55	1.97	80.2	1.32
10	triplet	2.63	2.68	1.88	90.5	1.49
11	singlet	2.57	2.55	1.89	86.1	1.41

[a] The N−N distances for **1**−**6** are for N atoms trans to the Ni atom. The N−N distances for **8**−**11** are for N atoms that belong to the same tridentate ligand. The N−N distances for ligands are defined as in the corresponding complexes. The N−Ni−N angles for **1**−**6** involve N atoms cis to the Ni atom. The N−Ni−N angles for **8**−**11** involve N atoms that belong to the same ligand.

We study separately the NLs. The tetradentate ligands in **1**−**6** are optimized as dianions, whereas the tridentate ligands in **8**−**11** are optimized as monoanions. We also perform geometry optimization of all NLs as neutral molecules. Both the dianionic and the neutral NLs of **2**, **5**, and **6** have cup shapes that resemble calixarenes. We use the results for the analysis of the geometrical changes caused by the metal coordination and for the calculation of the heterolytic and homolytic binding energies.

Ground States. For all complexes and NLs with an even number of electrons, we determine the ground electronic state among the closed-shell singlet, open-shell singlet, triplet, and quintet states. For systems with an odd number of electrons, such as **7**, **9**, the anionic NL of **11**, and the neutral NL of **10**, the ground electronic state is either the open-shell doublet or quartet state. The closed-shell and open-shell calculations are performed by using the restricted and unrestricted B3LYP, respectively.

For the first group of complexes, the results listed in Table 1 show that **1**−**3**, **5**, and **6** have closed-shell singlet ground states, whereas **4** has an open-shell triplet ground state. The closed-shell singlet ground state of **1** is in agreement with the experimental observations.[20] The open-shell triplet state energies of complexes **1**, **2**, and **3** are 1.3, 1.1, and 0.2 eV higher than the respective closed-shell singlet ground-state energies. However, for **4**−**6** the differences between the lowest lying triplet and singlet states are only about 0.05 eV.

In the second group, the four-coordinate complexes **8** and **9** have open-shell quintet and quartet ground states, respectively. The quartet ground state of **9** arises from the odd number of electrons in the neutral complex. Similarly, the pure carbon cone **7** has an odd number of electrons and a doublet ground state. The octahedral complexes **10** and **11** have open-shell triplet and closed-shell singlet ground states, respectively. The ground-state energies of **8**−**11** complexes are at least 0.1 eV lower than the lowest lying states of different multiplicity.

We also evaluate the spin purity of these ground electronic states, determined by the percent spin contamination $[\langle S^2\rangle - S(S+1)]100/[S(S+1)]$. The $\langle S^2\rangle$ values are obtained as part of the geometry optimization output, while the $S(S+1)$ values are 0.75, 2.00, 3.75, and 6.00 for doublet, triplet, quartet, and quintet spin states, respectively. The percent spin contamination

is considered acceptable when it is less than 10%. For the triplet ground states of complexes **4** and **10**, the values of the spin contamination are 0.5% and 5%, respectively. The doublet pure carbon cone **7** has a spin contamination of 5%. The spin contamination is 1% for each of the quartet **9** and quintet **8**. These results show that the ground-state spin multiplicities listed in Table 1 are rather pure.

The anionic NLs ground states affect the ground states of the corresponding complexes. The anionic ligands of **1**−**3** and **6** have closed-shell singlet ground states, whereas these of **4**, **5**, and **10** have open-shell triplet ground states. Thus, the large anionic NLs of **4** and **10** form high spin complexes. The anionic NL of **11** has an odd number of electrons and an open-shell doublet ground state. The neutral NLs are optimized in closed-shell singlet state for **1**−**6** and **10**, and in the open-shell doublet state for **11**. The different ground electronic states and the energetic closeness of states with different multiplicity could make these structures useful for magnetic applications.

Geometry Optimization. In a recent review, Ewels et al. have discussed several possible atomic configurations for the nitrogen doping of carbon nanostructures.[21] Zapol et al. also studied the effects of carbon ad-dimers on the electronic structure of CNTs.[22] Geometry optimization with DFT shows that substitutions of C with N atoms in CNTs lead to less than 0.02 Å shifts in the atomic positions.[21,23] Nitrogen atoms bonded to two and three C atoms in CNT have also been observed experimentally.[24] These authors also show by ab initio calculations that N atoms bonded to two C atoms form three stable pyridine-like substitution sites and vacancies in the walls of CNT. Here, we functionalize these nitrogen-doping sites and vacancies with transition metal atoms.

In Table 1, we list selected structural parameters obtained from the ground-state geometry optimization of the complexes shown in Figure 1 and the related anionic NLs. Our results are obtained with the B3LYP functional,[25,26] which is successful in accounting for the relative changes in metal−ligand distances.[27,28] The NLs with extended π-structures are relatively rigid and undergo small geometrical changes upon metal coordination, mostly observable at the N atom positions. These changes can be quantitatively evaluated from the relative changes in the N−N distance trans to the Ni atom. For our reference metalloporphyrin system **1**, this N−N distance decreases from 4.17 Å for the ligand to 3.94 Å for the complex, i.e., by 5.5%. Larger relative changes of 6.3% and 8.9% occur only for cones **3** and **5**, respectively. The tridentate NLs undergo even smaller relative changes than the tetradentate NLs.

We also study the Ni−N distances and N−Ni−N angles, connecting neighboring N atoms, in these complexes and present the results in Table 1. In the first group of complexes, we can find large structural variations. Complexes **1** and **4** are planar, as shown by the N−Ni−N angle of 90°, and have Ni−N distances of 1.97 and 1.96 Å, respectively. The Ni−N distance and N−Ni−N angle for the Ni(II)porphyrin **1** have been determined at 1.95 Å and 90.0°, respectively, using X-ray crystallography.[29] The calculated N−Ni−N angle of **1** is in excellent agreement with the experimental value, whereas the calculated Ni−N distance is 0.02 Å longer than the experimental one. In complex **5**, the Ni atom lies approximately in the plane of the four N atoms, similar to complexes **1** and **4**. This makes complex **5** almost square planar, although its NL is bowl-shaped. Despite the fact that the N−N distance of **5** undergoes the largest relative shortening upon complexation, the Ni−N distance of 2.00 Å in complex **5** is still the longest.

In complex **2**, the removal of the four methine linkers causes large buckling, reflected in the N−Ni−N angle of 87.1° and the shortest Ni−N bond of 1.83 Å. In cone **3**, the two unit cells of (4,4) CNT form a rigid carbon π-system that deforms the tetrapyrrole cap and causes an increase of the trans N−N distance relative to **2**. This deformation results in the Ni−N bond elongation of 0.09 Å in **3** relative to **2**, while the degree of buckling in these two structures is the same. In complex **6**, both the N−Ni−N angle and the Ni−N distance are similar to **2**. The buckling effect in complexes **2**, **3**, and **6** represents a displacement of the metal atom above the NNNN plane and a pyramidal distortion of the square planar complex.

This distortion breaks the square planar symmetry and allows for axial binding of a fifth ligand to the metal atom and the formation of a square pyramidal complex. The axial ligand binding is favored because the complex is already "pre-bent". This effect is similar to the "pre-bending" proposed for the synthesis of buckybowls.[30] In our buckled complexes, the smaller the value of the N−Ni−N angle is, the easier it is to bind another ligand. A convenient way to decrease this angle is to coordinate a larger transition metal ion. For example, the substitution of Ni(II) for Ru(II) in cone **2** causes a decrease of the buckling angle to 77.5°. Thus, cones **2** and **3** with Ru(II) on the tip have the potential to coordinate bidentate ligands, such as 2,2′-bipyridine.

In the second group of complexes, the Ni−N bonds in the four-coordinate **8** and **9** are as long as those in the Ni(II)-porphyrin. The N−Ni−N angles of **8** and **9** are smaller than 109.3° for a regular tetrahedron because of the rigid tridentate NLs. These four-coordinate complexes are functionalized with cyanide ligands. The substitution of other strong-field ligands for cyanide represents a feasible pathway for functionalization. On the other hand, our attempts to optimize four-coordinate complexes containing weaker-field ligands, such as chloride, ammonia, and water, instead of cyanide have produced unstable species. This is because the strong ligand field provided by the electron-rich nitrogen-doped NLs generally favors the binding of another strong-field ligand, such as cyanide, rather than a weaker field ligand.[10]

The octahedral complexes **10** and **11** feature the Ni−N distances of 1.88 and 1.89 Å, respectively. The N−Ni−N angles are close to 90°, as expected for the octahedral geometry. The spatial arrangement of the coordinating N atoms in the octahedral complexes **10** and **11** is structurally similar to that of the triazacycloalkane Ni(II) complexes,[31] but the N−Ni−N angle of 86.1° for complex **11** shows a smaller distortion from the octahedral symmetry than in $[Ni(1,4,7\text{-triazacyclononane})_2]^{2+}$ having the angle of 82°. Therefore, the optimized geometries of the two octahedral complexes with two NLs have low steric strain. Ligand substitution in these complexes is not favorable because the chelate effect of the tridentate NLs strengthens the Ni−NL bond. Cone **7** is structurally analogous to cone **9** where the cyanide ligand is removed.

In Table 1, we also show the Ni atom charges. They increase from the first to the second group of complexes. Within the first group of complexes, the charges slightly decrease along the rows in Figure 1, from the flat **1** and **4** to the buckled **3** and **6**, respectively. This decrease of the Ni atom charge correlates with the decrease of both the N−Ni−N angle and the NL size, seen in Figure 1. In complex **2**, the Ni charge decreases by 0.17 relative to the Ni(II)porphyrin **1**, as we reduce the ligand size and introduce buckling. In complex **3**, the Ni charge increases by 0.09 relative to **2**, as we increase the NL size. These results could help to determine which NLs form cones that are more

TABLE 2: Nickel−Ligand Total Binding Energies E_{b1} and E_{b2}, HOMO-LUMO Gaps for the Dianionic Ligand, and the Neutral Complex, as Well as EA and IP Values[a]

complex	E_{b1}	E_{b2}	$E_{gap}(L^{2+})$	$E_{gap}(cx)$	EA	IP
1	−12.00	−34.25	2.51	3.12	−1.06	6.71
2	−11.61	−33.90	2.52	2.35	−1.70	6.78
3	−9.21	−30.62	1.27	1.86	−2.76	6.35
4	−12.14	−32.91	2.61	3.03	−3.15	6.12
5	−10.87	−31.56	2.69	0.95	−3.08	6.08
6	−7.72	−32.64	1.13	1.20	−1.50	5.00
7				1.71	−2.66	7.03
8	−12.52	−30.26	1.26	1.17	−3.48	6.69
9	−11.09	−30.45	1.53	2.05	−2.21	6.34
10	−13.7	−32.07	1.26	0.94	−3.07	5.72
11	−10.38	−32.02	1.53	1.83	−1.42	5.26

[a] The HOMO-LUMO gaps of open-shell systems are determined relative to LUMOs of the same spin type as the HOMOs. All energies are in eV.

convenient for functionalization. Since higher metal atom charges lead to the formation of stronger axial bonds, complexes with larger NLs might be better candidates. This effect shows that the conjugated system acts as an electron sink. Of the complexes in the first group, the planar complex **4** seems to be best for functionalization.

In the second group of complexes, the Ni atomic charges also increase as the conjugated carbon systems increase in size. This can be seen when comparing **9** and **11**, which contain a smaller cone, to **8** and **10**, respectively, which contain a larger cone. In cone **7**, the natural charge at the cone tip carbon atom, which represents the first layer, is +0.12 e, while atoms of the second, third, and fourth layers have charges of −0.06, +0.01, and −0.06 e, respectively.

Metal−Ligand Binding Energies. The metal−ligand bond dissociation energies are crucial for the stability of all the complexes. We calculate these energies for homolytic (E_{b1}) and heterolytic (E_{b2}) dissociation, where the first means dissociation yielding neutral metal and ligand, whereas the second is for dissociation yielding Ni^{2+} and NL^{2-}:

$$E_{b1} = E(n) - E(L) - E(Ni) - E(CN)$$

$$E_{b2} = E(n) - E(L^{m-}) - E(Ni^{2+}) - E(CN^{-}) \qquad (1)$$

Here, $E(n)$ is the total energy of complex n, $E(L)$ and $E(L^{m-})$ are the total energies of the neutral and anionic ligands, respectively ($m = 1$ for complexes **8**−**11**, $m = 2$ for complexes **1**−**6**), $E(Ni)$ and $E(Ni^{2+})$ are the total energies of singlet Ni atom and singlet Ni^{2+}, respectively, and $E(CN)$ and $E(CN^{-})$ (nonzero for **8** and **9**) are the energies of doublet CN^0 and singlet CN^-, respectively. These energies are obtained for the optimized geometries of the structures. Thus, the energy changes arising from the changes in geometry that occur as a result of the bonding are included in both the homolytic and the heterolytic bond dissociation energies.

From Table 2, we can see that the values of E_{b2} are 3−4 times larger than those of E_{b1}, because the former also accounts for the $Ni^{2+}-L^{m-}$ electrostatic attraction. We found that the homolytic bond dissociation energy E_{b1} of the Ni(II)porphyrin calculated with the triple-ζ 6-311G* basis set in Gaussian03 is 1.9 eV higher than the value reported with use of the TZP basis set in the ADF software package.[12] We obtain a difference of 10−20% between these two approaches also for the other cones. Here, we focus on the relative changes in the binding energy that reflect the changes in their structure.

For the first group of complexes, E_{b1} decreases in size along the rows of Figure 1, showing weaker M−L bonds for the buckled complexes, relative to the planar complexes. The heterolytic E_{b2} decreases along the first two rows of complexes in a similar way. For complex **6**, we obtain a relatively low E_{b1}, due to a different degree of electronic structure stabilization upon homolytic binding. The neutral ligand of **6** has the lowest lying HOMO and the dianionic ligand has the highest lying HOMO energy, relative to the rest of the first group ligands. The buckled structures with weaker M−L binding have higher potential toward binding of a fifth ligand.

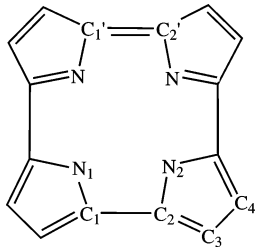

Figure 2. Diagram of the dianionic ligand of complex **2**.

For the second group of complexes, the E_{b1} values in **8** and **10** are higher than those in **9** and **11**, respectively, because the tridentate ligand in the first pair provides larger N−Ni−N angles. The largest value of E_{b1} is obtained for complex **10** that has a N−Ni−N angle of 90°, as required for the octahedral geometry. The heterolytic bond dissociation energies of the octahedral complexes are higher than those in the four-coordinate ones because of the more efficient bonding.

Stability of the Metal-Doped Cones. The above results show that the complexes of the second group do not possess significant steric strain. Therefore, we will discuss cone **2** in the first group, which is probably the least stable. Here, the steric strain caused by the buckling is the strongest, since the methine linkers are removed and stabilization by the extended conjugated system is also absent. To understand the stability of this complex, we address first the aromaticity of its dianionic ligand, shown in Figure 2.

In Figure 2, we have 18 π-electrons presented by the 9 π-bonds and 4 π-electrons from the lone pairs of the N_1 and N_2 atoms, or a total of 22 π-electrons. The π-electron count shows that the ligand is aromatic, as it fulfills the $4n + 2$ rule, where n is a positive integer. The optimized structure of the ligand is buckled with a conformation similar to that of complex **2** from Figure 1. Buckled aromatic compounds have a high degree of strain, due to the pyramidalization of the sp^2 carbon atoms. The experimental preparation of such structures is a synthetic challenge. Recently, several experimental approaches have been successfully developed for the synthesis of highly strained buckled aromatic compounds as precursors of fullerenes and other nanostructures.[30]

We first evaluate the bond orders for the C_1-C_2 and C_3-C_4 bonds. Our geometry optimization results show that the four pyrrole−pyrrole bonds in Figure 2 are equivalent for both the ligand and the complex **2**. As shown in Figure 2, the dianionic ligand of complex **2** contains one double bond ($C_1'-C_2'$) and three single bonds, or a total of five bonds distributed over the four pyrrole−pyrrole distances. This makes a formal bond order of $5/4 = 1.25$. This formal bond order is in very good agreement with the calculated Wiberg bond orders of 1.23 and 1.19 for complex **2** and its dianionic ligand, respectively. The formal C_3-C_4 bond order of 1.50 is also in relatively good agreement with the calculated values of 1.59 and 1.61 for the complex and the ligand, respectively.

From Figure 1, it is obvious that the stability of the ligand of complex **2** is contingent upon the strength of the pyrrole−pyrrole

bond C_1-C_2. We calculate the homolytic cleavage energy of this bond as the difference between the energy of the neutral singlet ligand of **2** and the energy of the neutral linear tetrapyrrole in its triplet ground state. The obtained value of −3.6 eV shows that the cyclic ligand is stable. In the same way, we can calculate the homolytic cleavage energy of the dianionic ligand. We obtain the value of 1.8 eV, which shows that the Coulombic repulsion of the two electrons increases the clevage energy by 5.4 eV and the dianionic ligand is unstable. It becomes stabilized upon the coordination of Ni^{2+}. The energy of this stabilization is E_{b2} of −33.90 eV (Table 2) and offsets the unstability of the dianionic ligand. The dianionic ligand of **2** might be further stabilized by additional groups. In fact, the functionalization of the open CNT might be a feasible method of experimental preparation. A natural way to stabilize this structure is by the addition of (4,4) CNT unit cells, as shown in **3**. We can expect that the other complexes in Figure 1 are more stable than **2** because of the presence of extended π-aromatic structures.

Electron Affinity (EA) and Ionization Potential (IP). In Table 2, we also list the values of the EAs and IPs of the complexes, calculated from

$$\mathrm{EA} = E(\mathrm{anion}) - E(\mathrm{neutral})$$

$$\mathrm{IP} = E(\mathrm{cation}) - E(\mathrm{neutral}) \qquad (2)$$

where E(neutral), E(cation), and E(anion) are the total energies of the neutral complex and its cation and anion. The EA values are negative, showing that the conjugated C complexes are electrophyllic. In the first group, the EAs generally decrease with the increase of the cone size, indicating a stronger attraction of the electron to the larger π-delocalized systems. In the second group, the EAs of **8** and **10**, containing a larger ligand, are lower than the smaller analogues **9** and **11**, respectively. Our EA and IP values of −1.06 and 6.71 eV for the Ni(II)porphyrin **1** are lower by about 0.3 eV relative to −1.31 and 7.01 eV, respectively, reported by Liao et al.,[12] who also show that the addition of electron withdrawing phenyl groups to the porphyrin ligand causes a decrease in the values of both the EA and IP.

In Figure 3, we present the dependence of the calculated HOMO and LUMO energies on the IPs and EAs, respectively. Despite the large structural differences of our complexes, we obtain very good linear correlations between these parameters, with correlation factors R of 0.98 and −0.96 for the EA versus LUMO and IP versus HOMO dependencies, respectively. Similar linear relationships have been reported for representative atomic and molecular systems with both covalent and ionic bonds.[32] From these correlations, we can conclude that complexes **3**−**5** have higher potential toward the binding of electron-donating ligands than **1**, **2**, and **6**. This is because complexes **3**−**5** contain larger electron-withdrawing NLs relative to **1**, **2**, and **6**. Complex **6** that has the lowest IP and the highest lying HOMO also has the highest electron-donating ability.

Molecular Orbital Analysis. We can gain further understanding of these complexes and their activity toward axial ligand binding from the molecular orbital energy diagram shown in Figure 4. We choose our coordinate system so that the metal atom is at the origin. For the complexes of the first group, the x and y axes are parallel to the N−N lines trans to the metal atom. For the octahedral complexes, the x, y, and z axes are approximately parallel to the three N−N lines trans to the Ni atom. For the four-coordinate complexes, the Ni−C bond of cyanide is oriented along the (1,1,1) vector.

We focus our attention on the molecular orbitals that contain large Ni 3d orbital contributions, since these are related to the metal−ligand binding. For the first group of complexes, the $d_{x^2-y^2}$ orbitals take part in the formation of the metal−tetradentate ligand bonds, whereas the d_{z^2} orbitals are related to the metal−axial ligand binding. For square planar d^8 complexes, formed by Ni(II), the $d_{x^2-y^2}$ orbitals are unoccupied.

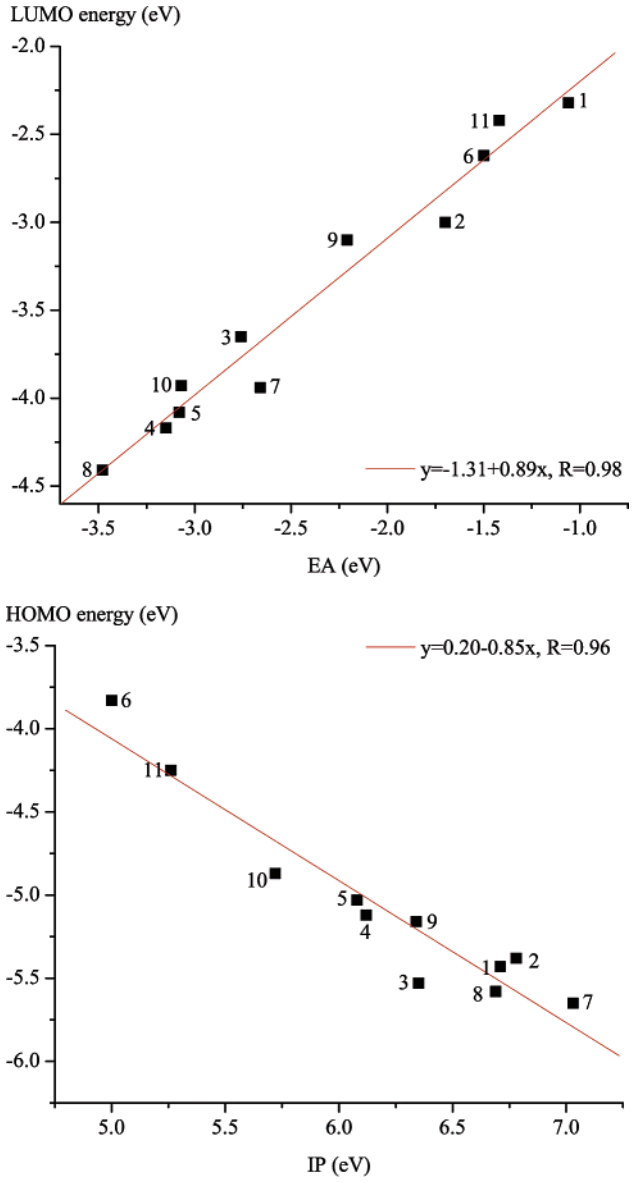

Figure 3. Dependence of the LUMO energies on the EAs (top) and the HOMO energies on the IPs (bottom) for the structures shown in Figure 1. The linear regression fitting results are given in the insets.

In Figure 4, we can notice some effects of buckling on the molecular orbital compositions for the first group of cones. For the buckled complexes **2**, **3**, and **6**, the $d_{x^2-y^2}$ percent contributions are lower than these of the planar complexes **1**, **4**, and **5**. This is because the buckling causes the displacement of the ligand N atoms along the z axis and decreases the $d_{x^2-y^2}$ orbital contribution. The HOMOs and HOMOs-1 of complexes **2** and **3** contain d_{xz} and d_{yz} orbital contributions of 25% and 12%, respectively. The increase in the d_{xz} and d_{yz} orbital energies of **2** and **3** relative to **1** is associated with the orientaion of the Ni−N bonds in **2** and **3** partially toward the d_{xz} and d_{yz} orbitals. For complexes **1**−**3** the d_{z^2} percent contributions also increase from 62% to 68%. These buckling-induced effects can change the strength of axial binding of potential ligands to the cones.

To follow this idea, we show in Figure 5 the schematic diagrams of the molecular orbitals with major d_{z^2} atomic orbital

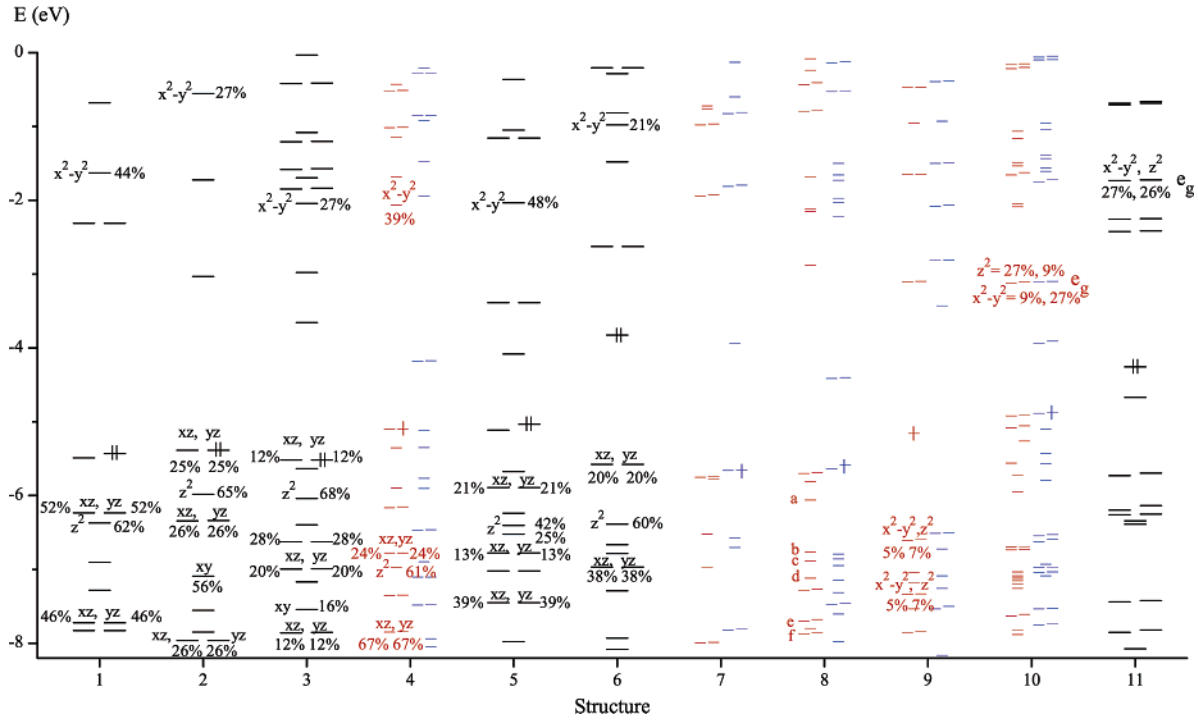

Figure 4. Molecular orbital energy levels of the ground states of the structures from Figure 1. The energy levels of closed shell systems are depicted with black horizontal lines. For open-shell systems, the α (spin up) and β (spin down) molecular orbital energy levels are shown as lighter lines on the left and right of the complexes, respectively. For the molecular orbitals with Ni d atomic orbital contributions higher than 5%, we note the percent contributions. Molecular orbital occupancies are indicated by vertical lines for the HOMOs only. The lower lying molecular orbitals of the closed-shell and open-shell systems are doubly and singly occupied, respectively. In the states of cone **8**, the populations are a = 5% of d_{yz}; b = 12% of d_{xz}; c = 7% of d_{z^2}, 5% of d_{yz}, and 5% of $d_{x^2-y^2}$; d = 7% of d_{z^2}; e = 6% of $d_{x^2-y^2}$; and f = 5% of $d_{x^2-y^2}$.

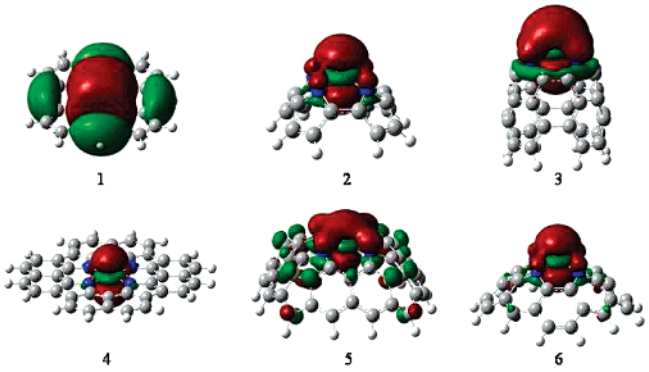

Figure 5. Schematic diagrams of the molecular orbitals that contain major Ni d_{z^2} and s atomic orbital contributions for the complexes of the first group.

contributions for the complexes of the first group. They are labeled with d_{z^2} in Figure 4. The second largest contribution to these orbitals after d_{z^2} is from the Ni 4s atomic orbitals, and this contribution is larger for the buckled complexes than for the flat complexes. For the flat structures **1** and **4**, the Ni 4s atomic orbital contributions are 24% and 23%, respectively, while for the buckled structures **2** and **6**, they increase to 29% and 26%, respectively. We have shown elsewhere[27] that the Pt 6s atomic orbitals of the square planar $[Pt_2(\mu\text{-}P_2O_5H_2)_4]^{4-}$ complex form axial σ-bonds. Thus, in our buckled complexes, the Ni 4s orbitals might also have a potential for axial binding.

For the four-coordinate complexes of the second group, we obtain small contributions from d_{z^2} and $d_{x^2-y^2}$ orbitals, as shown in Figure 4. For the octahedral complexes **10** and **11**, we show comparable contributions from the unoccupied Ni e_g orbital set, which contains the Ni d_{z^2} and $d_{x^2-y^2}$ atomic orbitals. For complex **11**, the Ni e_g orbital set energy is ≈1.4 eV higher than that for **10**. Although we were not able to find a well-defined t_{2g} orbital set, from the above e_g orbital set energy shift, it seems that the crystal field splitting energy for **11** is higher than that for **10**, i.e., the smaller ligand provides a stronger ligand field.

The HOMO-LUMO energy gaps of the complexes and the ligands, listed also in Table 2, depend strongly on the character of the ground state. The dianionic ligands of **4** and **5** that have triplet ground states have the largest energy gaps. The energy gaps of our structures decrease as the size of the conjugated π-system size increases, similar to the conjugated porphyrin tapes.[14] Also, the energy gaps decrease as the buckling angle increases. These two effects are demonstrated by the decreasing energy gaps of the complexes from **1** to **2**, due to buckling, and from **2** to **3**, due to enlargement of the π-system. Similarly, for complexes **8**−**11**, the structures containing the larger cone have smaller energy gaps. The HOMO-LUMO gaps of the doublet carbon cone **7** and the structurally similar ligand of complex **9** differ by only 0.18 eV.

Axial Coordination to Complexes of the First Group. For the complexes of the first group, the deviation of the N−Ni−N angle from 90° is a measure of the pyramidal distortion from the square planar geometry. This distortion breaks the plane of symmetry and makes the transition metal coordinationally unsaturated, allowing it to bind different types of ligands. Thus, the buckled structures shown in Figure 1 have two different binding sites with different geometrical and electronic environment.

As we show in Figure 5, the buckling of the structure leads to an asymmetric distribution of the Ni 4s and 3d orbital lobes relative to a plane of symmetry that contains the Ni atom and is parallel to the NNNN plane. The different sizes of the metal orbital lobes mean a different electronic environment for ligands approaching from the top and from the bottom. Consequently, in principle cones **2**, **5**, and **6** can bind two axial ligands with different strength: one above and the other below. In complex

5, the two ligand binding sites have similar electronic structure but different geometries, because the bowl-shaped ligand does not allow equivalent binding of large ligands above and below this structure. Cone **3** binds only one ligand on top. The planar complexes **1** and **4** provide two equivalent binding sites.

To show the different axial binding modes, we optimize the geometries of dianionic complexes **2**, **5**, and **6** that contain two cyanide ligands coordinated at the two axial positions. The Ni−C bond lengths for cyanide ligands coordinated axially at the top and at the bottom of these complexes are (Ni−C_t) and (Ni−C_b), respectively. For complex **2**, we obtained a Ni−C_t bond length of 1.92 Å, which is shorter than the Ni−C_b bond length of 2.01 Å. For complexes **5** and **6** we found the opposite, namely that the Ni−C_t bond lengths of 1.95 and 1.89 Å are longer than the respective Ni−C_b bond lengths of 1.90 and 1.86 Å. These axial binding results show that nanocones with large π-systems form weaker bonds with π-ligands at the cone tip than inside the cone. Also, the axial ligand binding to cones with larger NL sizes, such as **5**, is stronger than that to cones with smaller NL, such as **6**.

Conclusions

The described metal-doped carbon nanocones might be experimentally prepared with various advanced techniques,[33] allowing substitutions of selected carbon atoms, or via a direct stepwise chemical synthesis. A single-step direct synthesis was, for example, used to prepare nanocapsules from pyrogallol[4]-arenes.[34] In the first step of such a synthetic approach, one could prepare an open capsule with nitrogenated rim. The opening can be realized by electron beam cutting or by etching in solution.[35] The subsequent nitrogenation can be done by using a transient arc discharge.[16] In the second step, we could coordinate the transition metal atom to the nitrogenated rim, which brings the N atoms closer by about 0.1 Å. The structures also might be prepared in a series of ring closure reactions, in analogy to the synthetic schemes of C_{60},[1] combined with the "molecular surgery" approach to the synthetic opening and closing of fullerenes.[36]

The introduction of transition metal atom binding sites into nonmetallic nanoscale materials has a great potential for producing nanosystems with novel functionality. Indeed, these metallopyrrol-capped carbon nanocones allow for the binding of important ligands. The increase of the nanocone size causes a decrese of the metal atom charge and enhances its ability to bind ligands through σ-donation and π-back-bonding. The carboneous skeleton of the complexes then provides posibilities for electronic controlling of the attached ligands.

The metal binding to various ligands can be optimized by introducing further B and N substitutions.[37] These novel types of cones, capsules, and tubes might be applied in chemistry, as controlable catalysts or drug carriers, and could form a large mosaic of universal building blocks ready for use in molecular electronics and nanoscale machinery. These systems form a bridge between traditional nanostructures and molecules encountered in organic chemistry and biochemistry, and should be of great interest for their potential role in future nanodevices.

Acknowledgment. This work was done with the use of the IBM P690 at the National Computational Science Alliance.

References and Notes

(1) Kroto, H. W.; Heath, J. R.; O'Brien, S. C.; Curl. R. F.; Smalley R. E. *Nature* (*London*) **1985**, *318*, 162.

(2) Iijima, S. *Nature* (*London*) **1991**, *354*, 56.

(3) Krishnan, A.; Dujardin, E.; Treacy, M.; Hugdahl, J.; Lynum, S.; Ebbesen, T. *Nature* (*London*) **1997**, *388*, 451.

(4) Dresselhaus, M. S.; Dresselhaus, G.; Eklund, P. C. *Science of Fullerenes and Carbon Nanotubes*; Academic Press Inc.: San Diego, CA, 1996.

(5) Král, P.; Tomanek, D. *Phys. Rev. Lett.* **1999**, *82*, 5373.

(6) Zheng, M.; Jagota, A.; Strano, M. S.; Santos, A. P.; Barone, P.; Chou, S. G.; Diner, B. A.; Dresselhaus, M. S.; Mclean, R. S.; Onoa, G. B.; Samsonidze, G. G.; Semke, E. D.; Usrey, M.; Walls, D. J. *Science* **2003**, *302*, 1545.

(7) Banerjee, S.; Hemraj-Benny, T.; Wong, S. S. *Adv. Mater.* **2005**, *17*, 17.

(8) Hashimoto, A.; Yorimitsu, H.; Ajima, K.; Suenaga, K.; Isobe, H.; Miyawaki, J.; Yudasaka, M.; Iijima, S.; Nakamura, E. *Proc. Natl. Acad. Sci.* **2004**, *101*, 8527.

(9) Geno, M. K.; Halpern, J. *J. Am. Chem. Soc.* **1987**, *109*, 1238.

(10) Sanders, J. K. M.; Bampos, N.; Clyde-Watson, Z.; Darling, S. L.; Hawley, J. C.; Kim, H.-J.; Mak, C. C.; Webb, S. J. In *The Porphyrin Handbook*; Kadish, K. M., Smith, K. M., Guilard, R., Eds.; Academic Press Inc.: San Diego, CA, 1999.

(11) Lever, A. B.; Wilshire, J. P. *Can. J. Chem.* **1976**, *54*, 2514.

(12) Liao, M.-S.; Scheiner, S. *J. Chem. Phys.* **2002** *117*, 205.

(13) Baerends, E. J.; Ricciardi, C.; Rosa A.; van Gisbergen, S. J. A. *Coord. Chem. Rev.* **2002**, *230*, 5.

(14) Tsuda, A.; Osuka, A. *Science* **2001**, *293*, 79−82.

(15) Harada, R.; Kojima, T. *Chem. Commun.* **2005**, *6*, 716.

(16) Ziegler, T. *Chem. Rev.* **1991**, *91*, 651.

(17) Frisch, M. J.; Trucks, G. W.; Schlegel, H. B.; Scuseria, G. E.; Robb, M. A.; Cheeseman, J. R.; Montgomery, J. A., Jr.; Vreven, T.; Kudin, K. N.; Burant, J. C.; Millam, J. M.; Iyengar, S. S.; Tomasi, J.; Barone, V.; Mennucci, B.; Cossi, M.; Scalmani, G.; Rega, N.; Petersson, G. A.; Nakatsuji, H.; Hada, M.; Ehara, M.; Toyota, K.; Fukuda, R.; Hasegawa, J.; Ishida, M.; Nakajima, T.; Honda, Y.; Kitao, O.; Nakai, H.; Klene, M.; Li, X.; Knox, J. E.; Hratchian, H. P.; Cross, J. B.; Bakken, V.; Adamo, C.; Jaramillo, J.; Gomperts, R.; Stratmann, R. E.; Yazyev, O.; Austin, A. J.; Cammi, R.; Pomelli, C.; Ochterski, J. W.; Ayala, P. Y.; Morokuma, K.; Voth, G. A.; Salvador, P.; Dannenberg, J. J.; Zakrzewski, V. G.; Dapprich, S.; Daniels, A. D.; Strain, M. C.; Farkas, O.; Malick, D. K.; Rabuck, A. D.; Raghavachari, K.; Foresman, J. B.; Ortiz, J. V.; Cui, Q.; Baboul, A. G.; Clifford, S.; Cioslowski, J.; Stefanov, B. B.; Liu, G.; Liashenko, A.; Piskorz, P.; Komaromi, I.; Martin, R. L.; Fox, D. J.; Keith, T.; Al-Laham, M. A.; Peng, C. Y.; Nanayakkara, A.; Challacombe, M.; Gill, P. M. W.; Johnson, B.; Chen, W.; Wong, M. W.; Gonzalez, C.; Pople, J. A. *Gaussian 03*, revision D.01; Gaussian, Inc.: Wallingford, CT, 2004.

(18) Glendening, E. D.; Reed, A. E.; Carpenter, J. E.; Wienhold, F. NBO version 3.1.

(19) (a) ADF program package, version 2003.01: Baerends, E. J.; Ellis, D. E.; Ros, P. *Chem. Phys.* **1973**, *2*, 41. (b) te Velde G.; Baerends, E. J. *J. Comput. Phys.* **1992**, *99*, 84.

(20) Subramanian, J. In *Porphyrins and Metalloporphyrins*; Smith, K. M., Ed.; Elsevier Scientific: Amsterdam, The Netherlands, 1975.

(21) Ewels, C. P.; Glerup, M. *J. Nanosci. Nanotechnol.* **2005**, *5*, 1−19.

(22) Sternberg, M.; Curtiss, L. A.; Gruen, D. M.; Kedziora, G.; Horner, D. A.; Redfern, P. C.; Zapol, P. *Phys. Rev. Lett.* **2006**, *96*, 075506.

(23) Yi, J.-Y.; Bernholc, J. *Phys. Rev. B* **1993**, *47*, 1708.

(24) Terrones, M.; Ajayan, P. M.; Banhart, F.; Blase, X.; Carroll, D. L.; Charlier, J.-C.; Czerw, R.; Foley, B.; Grobert, N.; Kamalakaran, R.; Rohler-Redlich, P.; Rühle, M.; Seeger, T.; Terrones, H. *Appl. Phys. A: Mater. Sci. Process.* **2002**, *74*, 355.

(25) Stoll, L. K.; Zgierski, Z.; Kozlowski, P. M. *J. Phys. Chem. A* **2002**, *106*, 170.

(26) (a) Rodrigues, J. H.; Wheeler, D. E.; McCusker, J. K. *J. Am. Chem. Soc.* **1998**, *120*, 12051. (b) Stoyanov, S. R.; Villegas, J. M.; Cruz, A. J.; Lockyear, L. L.; Reibenspies, J. H.; Rillema, D. P. *J. Chem. Theory Comput.* **2005**, *1*, 95.

(27) Stoyanov, S. R.; Villegas, J. M.; Rillema, D. P. *J. Phys. Chem. B* **2004**, *108*, 12175−12180.

(28) Musaev, D. G.; Morokuma, K. *Inorg. Chem.* **2004**, *43*, 7702.

(29) Jentzen, W.; Turowska-Tyrk, I.; Scheidt, W. R.; Shelnutt, J. A. *Inorg. Chem.* **1996**, *35*, 3559.

(30) Bodwell, G. J.; Fleming, J. J.; Mannion, M. R.; Miller, D. O. *J. Org. Chem.* **2000**, *65*, 5360.

(31) Zompa, L. J.; Margulis, T. N. *Inorg. Chim. Acta* **1978**, *28*, L157.

(32) Zhan, C.-G.; Nichols, J. A.; Dixon, D. A. *J. Phys. Chem. A* **2003**, *107*, 4184.

(33) Král, P. *Phys. Rev. B* **2002**, *66*, 241401R.

(34) Antesberger, J.; Cave, G. V. W.; Ferrarelli, M. C.; Heaven, M. W.; Raston, C. L.; Atwood, J. L. *Chem. Commun.* **2005**, *7*, 892.

(35) Wong, S.; Woolley, A.; Joselevich, E.; Lieber, C. *Chem. Phys. Lett.* **1999**, *306*, 219.

(36) Komatsu, K.; Murata M.; Murata, Y. *Science* **2005**, *307*, 238.

(37) Machado, M.; Piquini, P.; Mota, R. *Chem. Phys. Lett.* **2004**, *392*, 428.